

Unintentional high density p-type modulation doping of a GaAs/AlAs core-multi-shell nanowire

J. Jadczak,^{†,∇} P. Plochocka,^{*,†} A. Mitiglu,[†] I. Breslavetz,[¶] M. Royo,[§] A. Bertoni,[§]
G. Goldoni,[§] T. Smolenski,[#] P. Kossacki,[#] A. Kretinin,[@] Hadas Shtrikman,[@] and
D. K. Maude[†]

*Laboratoire National des Champs Magnétiques Intenses, CNRS-UJF-UPS-INSa, 143, avenue de
Rangueil, 31400 Toulouse, Institute of Applied Physics, Academiei Str. 5, Chisinau, MD-2028,
Republic of Moldova, Laboratoire National des Champs Magnétiques Intenses,
CNRS-UJF-UPS-INSa, 25, avenue de Martyrs, 38042 Grenoble, Institute for Nanoscience,
CNR-NANO S3, via Campi 213/A, 41125 Modena, Italy, Departament de Química Física I
Analítica, Universitat Jaume I, Av. Sos Baynat s/n, 12080 Castelló, Spain, Department of Physics,
Informatics and Mathematics, University of Modena and Reggio Emilia, Italy, Institute of
Experimental Physics, Faculty of Physics, University of Warsaw, Hoża 69, 00-681 Warsaw,
Poland, Department of Condensed Matter Physics, The Weizmann Institute of Science, Rehovot
76100, Israel, and School of Physics and Astronomy, University of Manchester, UK*

E-mail: paulina.plochocka@lncmi.cnrs.fr

Abstract

Achieving significant doping in GaAs/AlAs core/shell nanowires (NWs) is of considerable technological importance but remains a challenge due to the amphoteric behavior of the dopant atoms. Here we show that placing a narrow GaAs quantum well in the AlAs shell effectively getters residual carbon acceptors leading to an *unintentional* p-type doping. Magneto-optical studies of such a GaAs/AlAs core multi-shell NW reveal quantum confined emission. Theoretical calculations of NW electronic structure confirm quantum confinement of carriers at the core/shell interface due to the presence of ionized carbon acceptors in the 1 nm GaAs layer in the shell. Micro-photoluminescence in high magnetic field shows a clear signature of avoided crossings of the $n = 0$ Landau level emission line with the $n = 2$ Landau level TO phonon replica. The coupling is caused by the resonant hole-phonon interaction, which points to a large 2D hole density in the structure.

Keywords: GaAs core/shell nanowires, 2D confinement, resonant phonon coupling.

Semiconductor nanowires (NWs) represent a rapidly expanding field of research largely due to their great technological promise.¹⁻⁵ For example, transistor action has been demonstrated using carbon nanotubes and silicon nanowires,^{6,7} it has been suggested that indium phosphide nanowires can be used as building blocks in nanoscale electronics,⁸ and doped radial core-multi-shell NWs have good chances to find industrial applications as high efficiency solar cells.⁹⁻¹³ NWs with two dimensional (2D) carriers localized at the core/shell interface offer new perspectives in quantum

*To whom correspondence should be addressed

†Laboratoire National des Champs Magnétiques Intenses, CNRS-UJF-UPS-INSA, 143, avenue de Rangueil, 31400 Toulouse

‡Institute of Applied Physics, Academiei Str. 5, Chisinau, MD-2028, Republic of Moldova

§Laboratoire National des Champs Magnétiques Intenses, CNRS-UJF-UPS-INSA, 25, avenue de Martyrs, 38042 Grenoble

§Institute for Nanoscience, CNR-NANO S3, via Campi 213/A, 41125 Modena, Italy

||Departament de Química Física I Analítica, Universitat Jaume I, Av. Sos Baynat s/n, 12080 Castelló, Spain

⊥Department of Physics, Informatics and Mathematics, University of Modena and Reggio Emilia, Italy

#Institute of Experimental Physics, Faculty of Physics, University of Warsaw, Hoża 69, 00-681 Warsaw, Poland

@Department of Condensed Matter Physics, The Weizmann Institute of Science, Rehovot 76100, Israel

△School of Physics and Astronomy, University of Manchester, UK

▽Institute of Physics, Wrocław University of Technology, 50-370 Wrocław, Poland

electronics.⁴ However, to introduce carriers the control and understanding of the doping mechanisms in NWs is crucial.

Epitaxial GaAs has been investigated for more than 40 years, a field of research propelled by the discovery of the quantum Hall effect with its panoply of exotic many body ground states.^{14,15} Significant efforts have been made to obtain high mobility 2D carriers in GaAs heterostructures grown by molecular beam epitaxy (MBE). Notably, the development of remote or modulation doping, which spatially separates the carriers from the dopant atoms, was a crucial step in the discovery of the fractional quantum Hall effect.¹⁵ The direct application of the modulation doping techniques to GaAs/AlAs NWs would seem to be a natural evolution. Today high quality GaAs/AlAs nanowires with a large aspect ratio and typical diameters of a few tens of nanometers are routinely grown by MBE using the vapour-liquid-solid (VLS) method.¹⁶⁻²⁴ While core multi-shell NWs would seem to be ideally suited for modulation doping, in practice achieving a significant doping remains a challenge. In the VLS method, depending upon the growth plane, dopants can act as donors or acceptors²⁵ and the dopant incorporation can be different for axial and lateral (sidewall) growth²⁶ resulting in an inhomogeneous dopant distribution, or even compensation and negligible doping.²⁷ In NWs the use of the AlGaAs ternary alloy for the shell can lead to the segregation of the Ga and Al atoms leading to the formation of the quantum dots.^{28,29} Moreover, using AlGaAs for the shell leads to a red shift of the photoluminescence emission from the NW core, which is not understood.³⁰ On the other hand both experiment and theory suggest that modulation doping in core-multi-shell NWs can lead to non uniform charge distribution with an accumulation of charge at the facets or corners of the hexagonal NW which can lead to quantum confinement.³¹

In this work, we show that incorporating a narrow GaAs quantum well, which can be used to accommodate dopants, in the AlAs shell of the NW can lead to significant unintentional p-type doping due to the incorporation of residual carbon acceptors. Experiment and calculations demonstrate that charge transfer at low temperature leads to quantum confinement with the formation of a *high density* two dimensional hole gas at the core/shell interface of the NW.

The GaAs/AlAs NWs were grown by MBE using the self-assisted VLS method, on (111)-

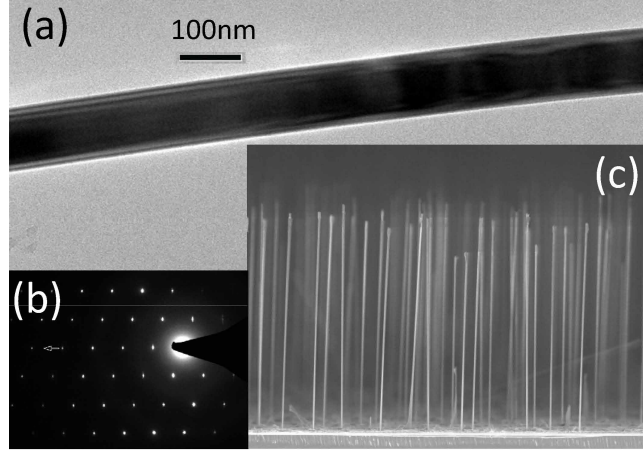


Figure 1: (a) typical transmission electron microscopy (TEM) image taken from the center of a GaAs/AlAs core-multi-shell NW, (b) pure zinc blende structure confirmed by the electron diffraction taken from the [011] direction, the arrow is aligned along the [111] growth direction, (c) scanning electron microscope (SEM) image of the GaAs/AlAs core-multi-shell NWs $\sim 11\mu\text{m}$ long.

oriented silicon bearing a native oxide layer. After water removal at 200°C , the Si wafer was outgassed in a separate chamber (600°C), before being transferred into the MBE growth chamber. Growth was initiated by Ga condensation at pin holes in the SiO_2 layer and carried out at 640°C and a group V/III (As_4/Ga) ratio of 100. Uniform diameter GaAs NWs were grown with a high aspect ratio, no significant tapering and pure zinc-blende structure, as revealed by careful transmission and scanning electron microscopy (Fig. 1(a) and (c)) and electron diffraction taken from the [011] direction (Fig. 1(b)). For growth of the shell (nominally AlAs 3 nm/GaAs 1 nm/ AlAs 3 nm) and 12 nm GaAs capping layer, the temperature was lowered to 520°C . The hexagonal GaAs NW core of side length $d \simeq 22\text{ nm}$ composes a substrate for the multilayer structure, which consists of a AlAs/GaAs/AlAs shell of a nominal thickness of 7 nm and a GaAs capping layer.

A typical μPL spectrum of a single core-multi-shell NW obtained in the absence of magnetic field at a temperature $T = 1.8\text{ K}$ is presented in Fig. 2 (see methods section for experimental details). For comparison, we show a μPL spectrum measured on a single core-shell NW.³² The structure of each sample is shown schematically in the inset of Fig. 2. We stress that both samples were grown in the same MBE chamber under nominally the same growth conditions. Both NWs have a rather large core (80 nm for core-shell and 60 nm for core-multi-shell) so that in a first

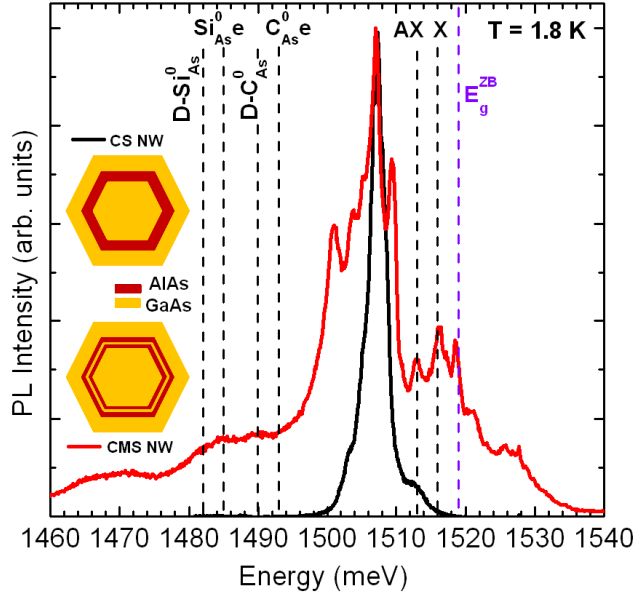


Figure 2: Typical μ PL spectra of core-shell GaAs/AlAs NW (black line) and core-multi-shell GaAs/AlAs (red line) excited by 660 nm laser line. Inset: schematic cross-section of core-shell and core-multi-shell NWs.

approximation quantum confinement can be neglected. The common feature of both emission spectra is the prominent peak at 1.507 eV with shoulders which develop into well resolved emission lines in a magnetic field.³² This transition is related to the so called KP series of excitons bound to defect pairs with different separations in extremely high quality epitaxial GaAs.³³ The emission energy of 1.507 eV corresponds well to the strongest line in the KP series in 1.504 – 1.511 eV spectral region.³⁴

The PL spectrum of the core-multi-shell NW is far richer than for the core-shell NW. In addition to the KP series, a large number of emission lines are resolved already in the zero magnetic field spectrum. At higher energies but still below the band gap of bulk GaAs ($E_g^{ZB} = 1.519$ eV) we can distinguish the free exciton (X) at 1.515 eV and exciton bound to neutral acceptor (AX) at 1.513 eV. Below the KP series, in the energy range 1.485 – 1.493 eV we observe a number of weak features with emission energies characteristic of the free-electron carbon-acceptor A^0e and the donor carbon-acceptor ($D^0 - A^0$) transitions.³⁵ This suggests that we have doped regions within the NW due to the unintentional incorporation of carbon. The shape of the spectra at low energy

is characteristic for p-doped structures, as recently observed for a single GaAs NW with an axial heterojunction.³⁶ In particular, it was shown that the emission energy for n-type and p-type material is quite different; for p-type GaAs NWs the emission is dominated by recombination via acceptor centers, whereas for n-type NWs emission is blue shifted with respect to the GaAs band gap due to a band filling effect with increasing doping concentration.^{36,37}

For the core-multi-shell NWs we observe additional emission lines at energies higher than the band gap of GaAs in the range 1.520 – 1.528 eV. This emission energy is typical for a GaAs quantum well (QW) of width 15 – 20 nm^{38,39} suggesting a quantum confinement of the carriers in the core. To distinguish this high energy emission from the emission in other spectral regions we refer to it a “2D like” in the rest of the paper. The core-multi-shell structure incorporates a 1 nm GaAs narrow quantum well in the AlAs shell at a distance of 3 nm from the core. No emission from this ultra thin quantum well (QW) is detected at higher energies, presumably due to the rapid thermalization (escape) of photo-created carriers. The 1 nm GaAs layer between the two AlAs layers is expected to getter impurities, notably residual carbon atoms.^{40,41} It acts as an efficient impurity trap due to the higher solubility of carbon atoms in GaAs and due to the floating of carbon atoms at the AlAs vacuum interface during the MBE growth.^{40,41} Moreover, for AlAs we expect the concentration of carbon to be quite high because Al atoms are more reactive with carbon or other impurities.⁴² For example, the residual carbon incorporation in AlAs can be two orders of magnitude higher than for GaAs.⁴² In our core-multi-shell NWs the carbon incorporated in the GaAs quantum well can lead to a non-uniform charge distribution with excess holes accumulated at the core/shell interface.

This hypothesis is confirmed by 3D self-consistent simulations of the NW electronic structure. The modeling assumes spatial invariance along the NW axis and includes the nominal multi-shell material modulation over the NW cross section. The interstitial GaAs quantum well is uniformly doped with a constant density of acceptors δ_A . Our results predict that a hole gas starts to accumulate at the core/shell interface for p-doping densities of the order of $2.0 \times 10^{19} \text{ cm}^{-3}$ (corresponding to a linear density of $4.63 \times 10^7 \text{ cm}^{-1}$ in the NW). The hole gas density distribution for a NW with

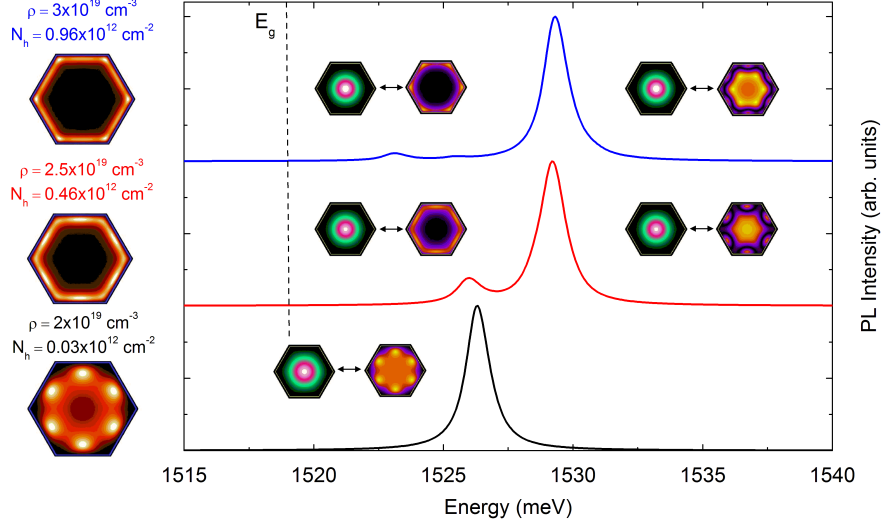


Figure 3: Calculated PL spectra (main panel) and hole gas distributions (small left panels) for core-multi-shell NWs with the p-doping densities ρ_A indicated in the left panels, together with the 2D free hole density N_h . The colormap insets illustrate the squared envelope functions for the electron (left) and hole (right) states whose recombination yields the PL peaks. The vertical dashed line indicates the position of the GaAs bulk band gap.

three selected doping densities is illustrated in the left panels of Fig. 3. The different localization patterns are in line with previous results.⁴³ At low densities the hole gas is distributed near the heterojunction forming six wide channels at the center of the hexagonal facets (bottom panel). As the doping density is increased the hole gas moves closer to the heterojunction and it forms, first, a quasi-uniform sixfold bent 2DEG (middle panel), and finally, six tunnel-coupled narrow channels at the edges (top panel).

The calculated PL spectra corresponding to the same doping densities can be seen in the main panel of Fig. 3. With increasing doping densities the exciton ground state red shifts and its intensity is substantially reduced. This can be explained as follows: The peak red shifts due to the larger attracting mean field experienced by the electron when the hole density is increased. At the same time, whereas the hole ground state is further localized near the heterojunction, the electron ground state remains in the center of the GaAs core (see two top-left insets in Fig. 3) due to the repulsive potential generated by the high density of acceptors. Therefore, the overlap between the ground electron and hole states becomes very small and the PL intensity of such transition is reduced. The

PL spectra of the NWs with higher acceptor densities show an additional intense peak at 1.529 eV. As illustrated in the corresponding insets in Fig. 3, this peak originates from the recombination of an electron in the ground state and a hole in an excited, but still occupied, state with an azimuthal-like nodal surface. Since this hole state is well spread over the center of the GaAs core it has a large overlap with the electron ground state leading to an intense peak in the PL spectrum. This peak is not observed at lower doping density since the excited hole state is unoccupied.

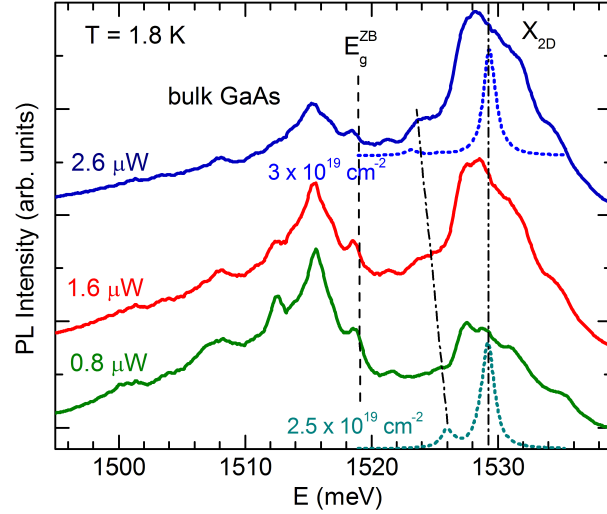


Figure 4: Evolution of the PL spectra (solid curves) of core-multi-shell GaAs/AlAs NW as function of the excitation power, at $T = 1.8$ K. The calculated PL spectra for different doping levels are plotted for comparison (dashed curves). The black dot-dashed lines are a guide to the eye to highlight the evolution of the position of 2D emission lines described in the text. Note that the spectra have been shifted vertically for clarity.

The concentration of photo created electron hole pairs, and thus the concentration of holes can also be tuned by varying the excitation power. A comparison between experimental results and theoretical simulation is presented in Fig. 4, which shows plots of μ PL spectra for different excitation powers. The relative intensity of the KP series of lines, below $E_g^{ZB} = 1.519$ eV, decreases as the excitation power increases. This is due to the saturation of these transitions when all the defect pairs have a bound exciton. In contrast, the 2D like emission intensity increases continuously with excitation power. For the highest excitation power, the spectra are dominated by emission related to the 2D hole gas. This further confirms the very different origins of each emission channel.

Theory predicts that the mechanism of the 2D recombination depends on the concentration

of photo-excited carriers. Increasing the number of photo created electron-hole pairs changes the overlap between electron and ground hole states due to the modified distribution of 2D hole gas in the core. The calculated PL spectra for two different hole concentrations are shown in Fig. 4 for comparison, showing qualitative agreement with the experimental data. The transition around 1.526 eV shifts toward lower energies with increasing excitation power, while the second peak around 1.529 eV, originated from recombination of electrons with holes in excited state, remains at the same energy. Its intensity is significantly enhanced as a straightforward consequence of the increased occupation of the electron and hole sub-bands involved in the radiative recombination.

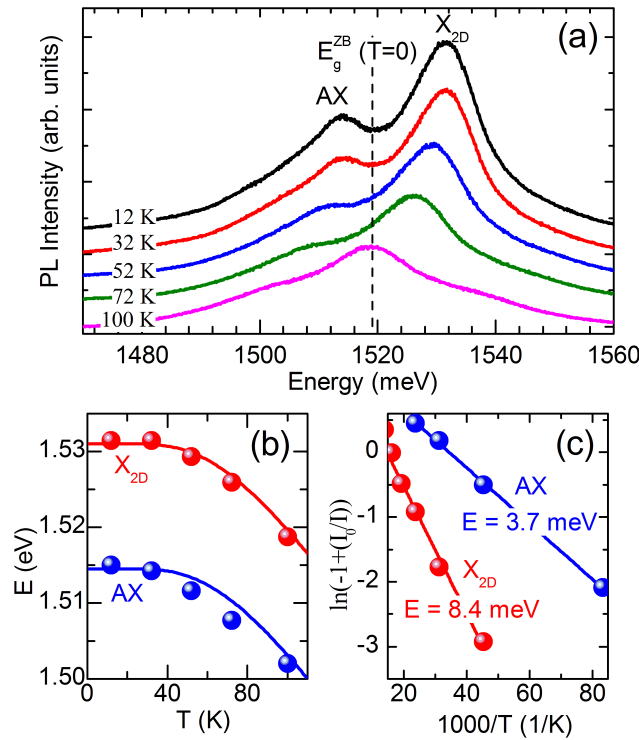


Figure 5: (a) Evolution of PL spectra of core-multi-shell GaAs/AlAs NW as a function of temperature, (b) Temperature dependence of the emission energy (symbols) together with the established temperature dependence of the GaAs band gap (lines) (c) Integrated PL intensity rate $\ln(-1 + I_0/I)$ as function of $1/T$ (symbols). The lines are the linear fits used to deduce the activation energies.

The temperature dependence of the μ PL spectra presented in Fig. 5 (a) provides further confirmation of the 2D character of the observed emission. In the μ PL spectra at $T=12$ K, two relatively broad peaks are observed corresponding to the recombination of the acceptor bound exciton (AX) and the confined 2D exciton (X_{2D}) at higher energies. Both shift to lower energy with increas-

ing temperature at a rate which tracks the temperature dependence of the GaAs band gap (see Fig. 5 (b)). The emission intensity of AX, observed below E_g^{ZB} , decreases much more rapidly than the intensity of the confined exciton peak indicative of a distinctly different dissociation channel for each transition. The thermal dissociation of excitons leads to a decrease in the normalized integrated emission intensity $I/I_0 = 1 + \alpha e^{-E/kT}$.⁴⁴ In order to estimate the activation energies associated with both processes, in Fig. 5 (b) we plot the integrated intensity rate $\ln(-1 + I_0/I)$ as function of $1/T$. The slope of the linear fit to the data gives the activation energies $E(AX) = 3.7$ meV and $E(X_{2D}) = 8.4$ meV. The activation energy for AX coincides with the binding energy of the acceptor bound exciton in high purity GaAs⁴⁴ and is also very close to the value reported earlier for ZB GaAs NWs (4 meV).¹⁶ The twofold higher activation energy of X_{2D} is expected for 2D confined excitons further confirming the localization of holes on the facets.

In Fig. 6 the color plot shows differential μ PL spectra, obtained by subtracting suitably averaged spectra, in magnetic fields up to 22 T applied perpendicular to the core-multi-shell NW growth axis. The PL emission lines sharpen and greatly increase in strength in a magnetic field, which allows us to resolve many more features. On top of the color plot the symbols (white stars) show the position of peaks manually identified for each spectra. This is useful to show weak features, particularly at low magnetic fields. At high energies we predominantly observe two lines corresponding to emission from quantum confined 2D carriers. At intermediate energies there is a series of lines previously identified with the KP series related to excitons bound to closely spaced defect pairs.³² At low energies, as we will later show, the observed lines can be identified with the LO and TO phonon replicas of the 2D emission observed at high energies.

For all the lines, at low magnetic field, the emission energy increases quadratically due to the diamagnetic shift. At higher magnetic field the dependence becomes linear in the Landau quantization regime. The magnetic field dependence of the KP series of lines in an undoped NW was discussed in detail in a previous publication.³² Here we focus on the lines linked to confined carrier emission. The energy of emission as a function of magnetic field can be described by the ground state of a 2D harmonic oscillator in perpendicular magnetic field,

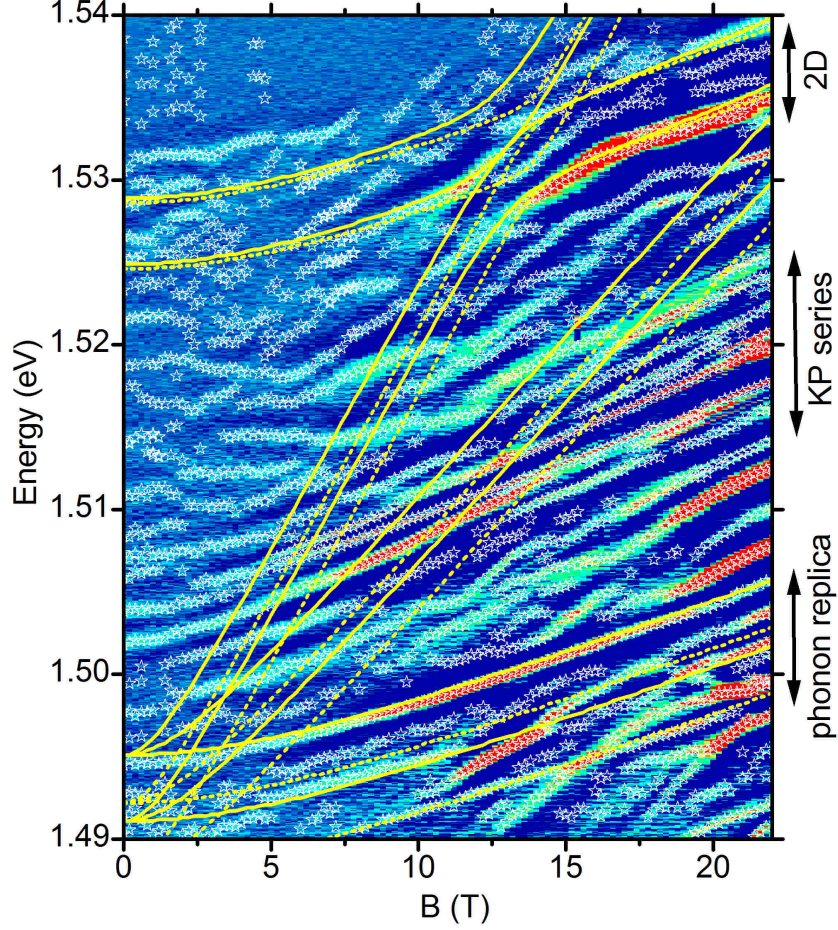


Figure 6: Color plot showing differential μ PL spectra of core-multi-shell GaAs/AlAs NW measured as function of magnetic field. The excitation power was a few nW and the temperature of the measurements was 1.7 K. The lines show the calculated evolution of the two high energy 2D emission lines together with their LO (dashed lines) and TO (solid lines) phonon replicas as described in the text. The observed avoided crossing is the result of resonant polaron coupling.

$$E(B) = E_0 + \hbar \sqrt{\omega_0^2 + (\omega_c/2)^2} \quad (1)$$

where ω_0 is the harmonic trap frequency, which controls the diamagnetic shift and $\omega_c = eB/m^*$ is the cyclotron frequency. Here we neglect the Zeeman splitting which is not resolved in our data. The LO and TO phonon replicas are given by $E(B) - \hbar\omega_{ph}$ where $\hbar\omega_{ph}$ is the LO or TO phonon energy in GaAs with $\hbar\omega_{LO} = 36.25$ meV or $\hbar\omega_{TO} = 33.29$ meV.⁴⁵ The 2D emission lines are quite weak at low magnetic field and the lower line shows distinct evidence for an avoided

crossing around 12 T which makes it difficult to fit Eq.(1) to the data. Fortunately, the phonon replicas have reasonable strength over a wide range of magnetic field allowing us to reliably extract $\hbar\omega_0 = 4.75$ meV and $m^* = 0.087m_e$. The second term in the Taylor expansion of Eq.(1) gives the coefficient for the diamagnetic shift $\hbar e^2/8\omega_0 m^{*2} \simeq 50\mu\text{eV/T}^2$ which is reasonable for a confined exciton.⁴⁶

Avoided crossings in the emission from the lowest ($n = 0$) Landau level have previously been observed in high density 2DEGs and are due to a resonant polaron coupling which occurs when $\Delta n\hbar\omega_c = \hbar\omega_{LO}$.⁴⁷ Occupancy arguments require that in order to observe such an effect the Fermi energy should be similar to or greater than the phonon energy, which requires a high 2D carrier density $\geq 1 \times 10^{12} \text{ cm}^{-2}$. The avoided crossing behavior can be described using a perturbation approach where the unperturbed energies are replaced by

$$E_{\pm} = \frac{1}{2} \left(E + E_{ph}^n \right) \pm \frac{1}{2} \sqrt{(E - E_{ph}^n)^2 - 4\gamma_{ph}^2} \quad (2)$$

where E_{ph}^n is the energy of the n^{th} phonon replica obtained from Eq.(1) with $\omega_c/2 \rightarrow (n + \frac{1}{2})\omega_c$ and γ_{ph} is the characteristic interaction energy for each phonon. The evolution of the emission lines, calculated using Eq.(2) and shown by the yellow lines in Fig. 6, is in good agreement with our data, nicely reproducing the phonon replicas and the avoided crossing behavior observed in the $n = 0$ Landau level. Note that as m^* and ω_0 were extracted from the unperturbed $n = 0$ phonon replica the only fitting parameters are the characteristic interaction energies (γ_{ph}) which we find to be equal to $\gamma_{TO} \simeq 4$ meV and $\gamma_{LO} \simeq 2$ meV. The avoided crossing with the $n = 1$ phonon replica exceeds our maximum magnetic field occurring for fields above 22 T. The observed avoided crossing occurs between the $n = 0$ Landau level emission and the $n = 2$ Landau level phonon replica. Moreover, the magnetic field position of the avoided crossing suggests that interaction with the TO phonon dominates. The interaction with the LO phonon would lead to an avoided crossing at higher magnetic field. This is further evidence for the 2D nature of the carriers involved since coupling to the TO phonon mode is absent in 3D systems.⁴⁸

In conclusion, we have carried out optical studies of the single GaAs/AlAs core-multi-shell NW

in high magnetic field. We have compared the obtained results with the typical spectra collected for single GaAs/AlAs core-shell NW with comparable diameter. In the PL spectra of the core-multi-shell NW we have observed emission above $E_g^{ZB} = 1.519$ eV which is related to 2D confinement of carriers in the core. Our results are in good agreement with theoretical calculations, which predict different localization regimes for carriers as a function of doping. Moreover, in magneto-PL spectra from core-multi-shell NWs we have observed avoided crossings of emission lines. The underlying coupling is caused by the hole-phonon interaction in a 2D system with a dense gas. This shows that the presence of 1 nm GaAs layer in the shell, which acts as an efficient impurity trap, can lead to the efficient incorporation of residual acceptors (carbon) and the formation of a dense 2D hole gas at the facets of the NW core.

Acknowledgement

We thank Ronit Popovitz-Biro for the careful TEM measurements. This work was partially supported by the Region Midi-Pyrénées, the Programme Investissements d’Avenir under the program ANR-11-IDEX-0002-02, reference ANR-10-LABX-0037-NEXT, ANR JCJC project milliPICS and project APOSTD/2013/052 Generalitat Valenciana Vali+d Grant. G.G. and A.B. acknowledge support from EU-FP7 Initial Training Network INDEX. G.G. acknowledges support from University of Modena and Reggio emilia, through grant ‘Nano- and emerging materials and systems for sustainable technologies’. We would also like to acknowledge partial support by the Israeli Science Foundation grant #530/08 and Israeli Ministry of Science grant #3-6799.

Supporting Information Available

Experimental techniques

The study of the optical properties of core-multi-shell NW’s was carried out in two experimental setups. For measurements of the micro-photoluminescence (μ PL) in magnetic field the sample was placed in a system composed of piezoelectric x-y-z translation stages and a microscope objective.

The μ PL system was cooled to a temperature of $T=1.8$ K in a cryostat placed in a resistive magnet producing magnetic fields of up to $B = 22$ T. The field was applied in the Faraday configuration, perpendicular to the NW $\langle 111 \rangle$ growth axis. The sample was illuminated by a diode laser at 660 nm. Both the exciting and collected light were transmitted through a monomode fiber coupled directly to the microscope objective. The diameter of the excitation beam on the sample was of the order of $1\ \mu\text{m}$. The emission from the sample was dispersed in a spectrometer equipped with a multichannel CCD camera. For additional μ PL measurements in the absence of magnetic field, the sample was placed in helium flow cryostat with optical access. The cryostat was mounted on motorized x-y translation stages. The μ PL was measured for temperatures varying from 10 to 100 K. Excitation and collection was implemented using a microscope objective with a numerical aperture $\text{NA}=0.66$ and magnification $\times 50$. The diameter of the excitation spot on the sample was of the order of $1\ \mu\text{m}$ and the μ PL spectra have been recorded using a spectrometer equipped with a multichannel CCD camera.

Structural properties of the GaAs/AlAs/GaAs/AlAs/GaAs core/shell QW nanowires

We do not have a structural characterization of the exact NW investigated in our μ PL set up. We provide in this section structural characterization and direct evidence for the presence of a well-defined QW within a very similar core multi shell structure grown in the same system and under similar growth conditions and layer thicknesses. This sample was studied intensively by cross sectional HR-TEM (prepared using FIB) as demonstrate in Figure 7. Figure 7(a) shows a HR-TEM image taken on a cross section of the multi shell nanowire showing the two AlAs shell layers (bright stripes) and a few monolayers thick GaAs QW embedded between them (GaAs core and capping layer on the right and left hand sides, respectively, the scale bar is 5 nm. Figure 7(b) is a full TEM image of the cross section taken from a core multi shell nanowire with very similar nominal thicknesses as the ones studied in this work. Figure 7(c) shows the intensity profile showing clearly the splitting of the AlAs layer into two layers, consistent with the presence of a thin GaAs QW in between them.

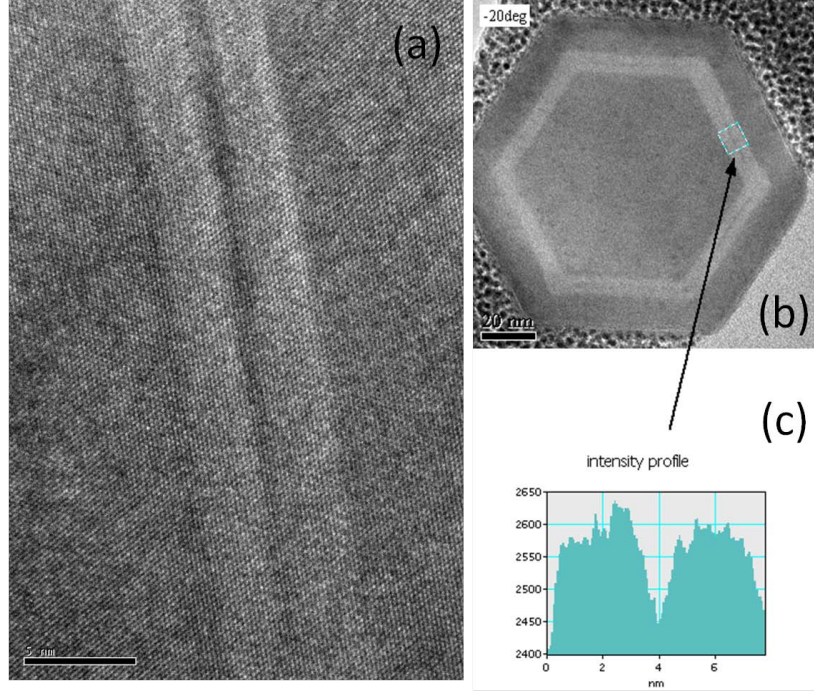


Figure 7: (a) HR-TEM image taken on a cross section of the multi shell nanowire showing the two AlAs shell layers (bright stripes) and a few monolayers thick GaAs QW embedded between them (GaAs core and capping layer on right and left hand sides, respectively, scale bar is 5 nm). (b) TEM image of a cross section taken from a core multi shell nanowire. (c) intensity profile of the region marked on the cross section.

Self consistent calculation of the charge distribution

Calculations have been conducted within a standard envelope function approach, in a single-band approximation. We consider the NW as a 3D system spatially invariant along the NW axis direction z . This allows us to factorize the electron (hole) envelope functions as $\Psi_{nk_z}^{e(h)}(\mathbf{r}, z) = \varphi_n^{e(h)}(\mathbf{r})e^{ik_z z}$, with parabolic energy dispersions, $E_{nk_z}^{e(h)} = \varepsilon_n^{e(h)} \pm \frac{\hbar^2 k_z^2}{2m_{e(h)}^z}$, in the in-wire momentum k_z . Over the $\mathbf{r} \equiv x, y$ plane, the NW cross section is hexagonal, and the material and doping modulations are described in a corresponding hexagonal domain using a symmetry-compliant triangular grid. We use an isotropic electron effective mass ($m_e^z = m_e^r$) but a highly anisotropic hole mass. Over the in-plane direction we use the hole mass along the $[110]$ direction which is much larger than the hole mass that we use along the in-wire direction $[111]$. The ground state hole density $n_h(r)$ is obtained through a Kohn-Sham LDA procedure.

The self-consistent potential $V_{KS}(r) = V(r) + V_H(r) + V_{XC}(r)$ includes the effect of the spatial

confinement $V(r)$ determined by the materials band offset, the Hartree potential $V_H(r)$ generated by free holes and static acceptors, and an approximate exchange-correlation potential $V_{XC}(r)$.⁴⁹ In our samples, conduction band electrons are generated by the laser pumping alone, thus they are minority carriers with a low density: we solve the corresponding Schrödinger equation including the electrostatic potential generated by the self-consistent hole density and the density of static acceptors. In this way we take into account excitonic effects at a mean-field level. Further details can be found in references.^{43,50}

From the conduction and valence band states, we compute the PL spectra neglecting dynamic screening effects and assuming that the photoexcited carriers relax to the lowest available state before the radiative recombination. This means that electrons recombine from the lowest-lying conduction states with holes in states lying above the Fermi level μ . The PL intensity is obtained as

$$\tau(\omega) \propto \sum_{im} |S_{im}|^2 \int \frac{dk_z}{2\pi} f^e(E_{ik_z}^e, T) (1 - f^h(E_{mk_z}^h - \mu, T)) \Gamma(E_{ik_z}^e - E_{mk_z}^h - \hbar\omega - \gamma), \quad (3)$$

where

$$S_{im} = \int d\mathbf{r} \phi_i^e(\mathbf{r}) \phi_m^h(\mathbf{r}) \quad (4)$$

is the overlap integral between a conduction band state i and a valence band state m , $f^{e(h)}$ is the electron (hole) Fermi occupation function at a given temperature T , and Γ is a Lorentzian function with a phenomenological bandwidth γ that we set to 1 meV in order to reproduce the width at half maximum of the experimental peaks. We use the material-dependent parameters indicated in Table 1, a temperature $T = 1.8$ K, and we assume that the 1 nm GaAs quantum well is uniformly doped with a constant density of completely ionized acceptors ρ_A . The Fermi level is placed 0.4 eV above the GaAs valence band edge following experimental observations in highly p-doped GaAs.⁵¹

Table 1: Material parameters employed in the numerical calculations extracted from reference.⁵² Band edges have been calculated assuming the (60:40) rule. Effective masses are taken along [111] direction for $m_z^{e,h}$ and [110] for $m_r^{e,h}$.⁵³

	GaAs	AlAs
Band gap E_g [eV]	1.519	3.02
Conduction band edge E_C [eV]	0.9114	1.812
Valence band edge E_V [eV]	-0.6076	-1.208
Electron effective masses m_z^e	0.0662	0.19
m_r^e	0.0662	0.19
Hole effective masses m_z^h	0.082	0.109
m_r^h	0.680	0.818

References

- (1) Hu, J.; Odom, T. W.; Lieber, C. M. *Accounts of Chemical Research* **1999**, 32, 435–445.
- (2) Cui, Y.; Lieber, C. M. *Science* **2001**, 291, 851.
- (3) Thelander, C. *Mater. Today* **2006**, 9, 28.
- (4) Lieber, C. M.; Wang, Z. L. *MRS Bulletin* **2007**, 32, 99–108.
- (5) Lu, W.; Lieber, C. M. *Nature Mater.* **2007**, 6, 841.
- (6) Tans, S. J.; Verschueren, A. R. M.; Dekker, C. *Nature* **1998**, 393, 49.
- (7) Cui, Y.; Zhong, Z.; Wang, D.; Wang, W. U.; Lieber, C. M. *Nano Letters* **2003**, 3, 149–152.
- (8) Duan, X.; Huang, Y.; Cui, Y.; Wang, J.; Lieber, C. M. *Nature* **2001**, 409, 66.
- (9) Krogstrup, P.; Jørgensen, H. I.; Heiss, M.; Demichel, O.; Holm, J. V.; Aagesen, M.; Nygard, J.; i Morral, A. F. *Nature Photonics* **2013**, 7, 306–310.
- (10) Spirkoska, D.; Fontcuberta i Morral, A.; Dufouleur, J.; Xie, Q.; Abstreiter, G. *physica status solidi (RRL) Rapid Research Letters* **2011**, 5, 353–355.

- (11) Fickenscher, M.; Shi, T.; Jackson, H. E.; Smith, L. M.; Yarrison-Rice, J. M.; Zheng, C.; Miller, P.; Etheridge, J.; Wong, B. M.; Gao, Q.; Deshpande, S.; Tan, H. H.; Jagadish, C. *Nano Letters* **2013**, *13*, 1016–1022.
- (12) Estrin, Y.; Rich, D. H.; Kretinin, A. V.; Shtrikman, H. *Nano Letters* **2013**, *13*, 1602–1610.
- (13) Fontcuberta i Morral, A.; Spirkoska, D.; Arbiol, J.; Heigoldt, M.; Morante, J. R.; Abstreiter, G. *Small* **2008**, *4*, 899–903.
- (14) Klitzing, K. v.; Dorda, G.; Pepper, M. *Phys. Rev. Lett.* **1980**, *45*, 494–497.
- (15) Tsui, D. C.; Stormer, H. L.; Gossard, A. C. *Phys. Rev. Lett.* **1982**, *48*, 1559–1562.
- (16) Titova, L. V.; Hoang, T. B.; Jackson, H. E.; Smith, L. M.; Yarrison-Rice, J. M.; Kim, Y.; Joyce, H. J.; Tan, H. H.; Jagadish, C. *Applied Physics Letters* **2006**, *89*, –.
- (17) Pistol, M.-E.; Pryor, C. E. *Phys. Rev. B* **2008**, *78*, 115319.
- (18) Shtrikman, H.; Popovitz-Biro, R.; Kretinin, A.; Heiblum, M. *Nano Letters* **2009**, *9*, 215–219.
- (19) Shtrikman, H.; Popovitz-Biro, R.; Kretinin, A.; Houben, L.; Heiblum, M.; Bukala, M.; Galicka, M.; Buczko, R.; Kacman, P. *Nano Letters* **2009**, *9*, 1506–1510, PMID: 19253998.
- (20) Spirkoska, D. et al. *Phys. Rev. B* **2009**, *80*, 245325.
- (21) Algra, R. E.; Hocevar, M.; Verheijen, M. A.; Zardo, I.; Immink, G. G. W.; van Enkevort, W. J. P.; Abstreiter, G.; Kouwenhoven, L. P.; Vlieg, E.; Bakkers, E. P. A. M. *Nano Letters* **2011**, *11*, 1690–1694.
- (22) Jahn, U.; Lähnemann, J.; Pfüller, C.; Brandt, O.; Breuer, S.; Jenichen, B.; Ramsteiner, M.; Geelhaar, L.; Riechert, H. *Phys. Rev. B* **2012**, *85*, 045323.
- (23) Musin, I. R.; Filler, M. A. *Nano Letters* **2012**, *12*, 3363–3368.

- (24) Assali, S.; Zardo, I.; Plissard, S.; Kriegner, D.; Verheijen, M. A.; Bauer, G.; Meijerink, A.; Belabbes, A.; Bechstedt, F.; Haverkort, J. E. M.; Bakkers, E. P. A. M. *Nano Letters* **2013**, *13*, 1559–1563.
- (25) Hilse, M.; Ramsteiner, M.; Breuer, S.; Geelhaar, L.; Riechert, H. *Applied Physics Letters* **2010**, *96*, –.
- (26) Dufouleur, J.; Colombo, C.; Garma, T.; Ketterer, B.; Uccelli, E.; Nicotra, M.; Fontcuberta i Morral, A. *Nano Letters* **2010**, *10*, 1734–1740.
- (27) Casadei, A.; Krogstrup, P.; Heiss, M.; Röhr, J. A.; Colombo, C.; Ruelle, T.; Upadhyay, S.; Sørensen, C. B.; Nygård, J.; Fontcuberta i Morral, A. *Applied Physics Letters* **2013**, *102*, –.
- (28) Heiss, M. et al. *Nature Materials* **2013**, *12*, 439.
- (29) Rudolph, D.; Funk, S.; Döblinger, M.; Morkötter, S.; Hertenberger, S.; Schweickert, L.; Becker, J.; Matich, S.; Bichler, M.; Spirkoska, D.; Zardo, I.; Finley, J. J.; Abstreiter, G.; Koblmüller, G. *Nano Letters* **2013**, *13*, 1522–1527.
- (30) Hocevar, M.; Thanh Giang, L. T.; Songmuang, R.; den Hertog, M.; Besombes, L.; Bleuse, J.; Niquet, Y.-M.; Pelekanos, N. T. *Applied Physics Letters* **2013**, *102*, –.
- (31) Funk, S. et al. *Nano Letters* **2013**, *13*, 6189–6196.
- (32) Plochocka, P.; Mitioglu, A. A.; Maude, D. K.; Rikken, G. L. J. A.; Granados del Aguila, A.; Christianen, P. C. M.; Kacman, P.; Shtrikman, H. *Nano Letters* **2013**, *13*, 2442–2447.
- (33) Kunzel, H.; Ploog, K. *Applied Physics Letters* **1980**, *37*, 416–418.
- (34) Skolnick, M. S.; Harris, T. D.; Tu, C. W.; Brennan, T. M.; Sturge, M. D. *Applied Physics Letters* **1985**, *46*, 427–429.
- (35) Pavesi, L.; Guzzi, M. *Journal of Applied Physics* **1994**, *75*, 4779–4842.

- (36) Sager, D.; Gutsche, C.; Prost, W.; Tegude, F.-J.; Bacher, G. *Journal of Applied Physics* **2013**, *113*, –.
- (37) Borghs, G.; Bhattacharyya, K.; Deneffe, K.; Van Mieghem, P.; Mertens, R. *Journal of Applied Physics* **1989**, *66*, 4381–4386.
- (38) Ferreira, A. C.; Holtz, P. O.; Sernelius, B. E.; Buyanova, I.; Monemar, B.; Mauritz, O.; Ekenberg, U.; Sundaram, M.; Campman, K.; Merz, J. L.; Gossard, A. C. *Phys. Rev. B* **1996**, *54*, 16989–16993.
- (39) Glasberg, S.; Shtrikman, H.; Bar-Joseph, I. *Phys. Rev. B* **2001**, *63*, 201308.
- (40) Meynadier, M. H.; Brum, J. A.; Delalande, C.; Voos, M.; Alexandre, F.; Liévin, J. L. *Journal of Applied Physics* **1985**, *58*, 4307–4312.
- (41) Petroff, P. M.; Miller, R. C.; Gossard, A. C.; Wiegmann, W. *Applied Physics Letters* **1984**, *44*, 217–219.
- (42) Tokumitsu, E.; Katoh, T.; Kimura, R.; Konagai, M.; Takahashi, K. *Japanese Journal of Applied Physics* **1986**, *25*, 1211–1215.
- (43) Bertoni, A.; Royo, M.; Mahawish, F.; Goldoni, G. *Phys. Rev. B* **2011**, *84*, 205323.
- (44) Bimberg, D.; Sondergeld, M.; Grobe, E. *Phys. Rev. B* **1971**, *4*, 3451–3455.
- (45) Adachi, S. *Journal of Applied Physics* **1985**, *58*, R1–R29.
- (46) Walck, S. N.; Reinecke, T. L. *Phys. Rev. B* **1998**, *57*, 9088–9096.
- (47) Harper, P. G.; Hodby, J. W.; Stradling, R. A. *Reports on Progress in Physics* **1973**, *36*, 1.
- (48) Butov, L. V.; Grinev, V. I.; Kulakovskii, V. D.; Andersson, T. G. *Phys. Rev. B* **1992**, *46*, 13627–13630.
- (49) Gunnarsson, O.; Lundqvist, B. I. *Phys. Rev. B* **1976**, *13*, 4274–4298.

- (50) Royo, M.; Bertoni, A.; Goldoni, G. *Phys. Rev. B* **2013**, 87, 115316.
- (51) Pashley, M. D.; Haberern, K. W.; Feenstra, R. M.; Kirchner, P. D. *Phys. Rev. B* **1993**, 48, 4612–4615.
- (52) Levinshtein, M.; Rumyantsev, S.; Shur, M. *Handbook series on semiconductor parameters Vol. 2*; World Scientific Publishing, 1996.
- (53) Fishman, G. *Phys. Rev. B* **1995**, 52, 11132–11143.

This material is available free of charge via the Internet at <http://pubs.acs.org/>.